Physica D 347 (2017) 12–20

Contents lists available at ScienceDirect

Physica D

journal homepage: www.elsevier.com/locate/physd

Hopf and Homoclinic bifurcations on the sliding vector field of switching systems in $\mathbb{R}^3$: A case study in power electronics

Rony Cristiano [a], Tiago Carvalho [b,*], Durval J. Tonon [c], Daniel J. Pagano [a]

[a] Department of Automation and Systems, Federal University of Santa Catarina, Florianópolis, Brazil
[b] FC–UNESP, CEP 17033–360, Bauru, São Paulo, Brazil
[c] Institute of Mathematics and Statistics of Federal University of Goiás, CEP 74001-970, Goiânia, Goiás, Brazil

HIGHLIGHTS

- A dc–dc boost converter with sliding mode control and washout filter is studied.
- A Hopf bifurcation is observed at the sliding vector field.
- A homoclinic loop appears for some choices on the parameters.

ARTICLE INFO

Article history:
Received 23 December 2015
Accepted 12 February 2017
Available online 24 February 2017
Communicated by G. Stepan

Keywords:
Filippov systems
Sliding Hopf bifurcation
Sliding Homoclinic bifurcation
Boost converter
Sliding mode control

ABSTRACT

In this paper, Hopf and homoclinic bifurcations that occur in the sliding vector field of switching systems in $\mathbb{R}^3$ are studied. In particular, a dc–dc boost converter with sliding mode control and washout filter is analyzed. This device is modeled as a three-dimensional Filippov system, characterized by the existence of sliding movement and restricted to the switching manifold. The operating point of the converter is a stable pseudo-equilibrium and it undergoes a subcritical Hopf bifurcation. Such a bifurcation occurs in the sliding vector field and creates, in this field, an unstable limit cycle. The limit cycle is connected to the switching manifold and disappears when it touches the visible–invisible two-fold point, resulting in a homoclinic loop which itself closes in this two-fold point. The study of these dynamic phenomena that can be found in different power electronic circuits controlled by sliding mode control strategies are relevant from the viewpoint of the global stability and robustness of the control design.

1. Introduction

Switching power electronic devices are strongly non-linear and can be modeled as piecewise smooth dynamical systems. It has been shown that this class of systems can exhibit various types of complex phenomena, including the classic bifurcations (Hopf, Saddle–Node, Homoclinic, etc.) and bifurcations induced by discontinuity [1].

In case where the dynamical system is discontinuous piecewise smooth, orbits can be confined to the switching manifold. This phenomenon is known as sliding motion and this class of systems is called as Filippov systems [2]. The occurrence of such a phenomenon has been reported in various applications involving sliding mode control. Here we highlight the applications in power electronics converters [3–7].

In this paper, we study the Hopf and Homoclinic bifurcations that appear in the sliding vector field of three-dimensional Filippov systems. For this study we consider the model of a dc–dc boost power electronics converter with sliding mode control and washout filter (SMC-Washout) to reject load changes [5]. These bifurcations on the sliding vector field are analogous to the standard continuous case, and will be called Sliding Hopf and Sliding Homoclinic bifurcations. However, sliding homoclinic bifurcations differ a little from the standard case, since the closing point of the homoclinic loop is not on a saddle equilibrium point, but in a visible–invisible two-fold singularity that has dynamics saddle in the sliding region. Moreover, the homoclinic bifurcation exhibited here is of codimension-one and is obtained when a single parameter is varied.

Dynamical systems that have a two-fold singularity possess a very rich and complex dynamics. In [8–11] two-fold singularities

* Corresponding author.
E-mail addresses: rony.cristiano@ufsc.br (R. Cristiano), tcarvalho@fc.unesp.br (T. Carvalho), djtonon@ufg.br (D.J. Tonon), daniel.pagano@ufsc.br (D.J. Pagano).

http://dx.doi.org/10.1016/j.physd.2017.02.005
0167-2789/

are studied and in [12,13] applications of such theory in electrical and control systems, respectively, are exhibited.

The Hopf bifurcation is a local bifurcation in which an equilibrium point of a smooth dynamical system loses stability when a pair of complex conjugate eigenvalues crosses the imaginary axis of the complex plane. In this case, an unstable limit cycle (subcritical Hopf) or stable (supercritical Hopf) arises from an equilibrium point.

The Homoclinic bifurcation is a global bifurcation that occurs when a limit cycle collides with a saddle equilibrium point. The existence of a homoclinic orbit implies global changes in system dynamics. On bidimensional systems studied by Andronov et al. [14], the existence of a homoclinic orbit causes the sudden appearance of a limit cycle with same stability of the homoclinic orbit. In the same way, we can say that Homoclinic bifurcation is the mechanism by which a limit cycle, created for example from a Hopf bifurcation, is destroyed. More details about the Hopf and Homoclinic bifurcation in smooth dynamical systems, can be found in [15–18].

In the literature there are several works on Homoclinic bifurcation and Hopf bifurcation analysis in nonsmooth dynamical systems [19–26], where the bifurcations studied are induced by the discontinuity. For example, in Kuznetsov et al. [24], are study "Pseudo-Homoclinic" bifurcations where a standard saddle equilibrium point may have a homoclinic loop containing a sliding segment. In Dercole et al. [23], a bifurcation of codimension 2 where a limit cycle that arises from an equilibrium point associated with a Boundary Equilibrium Bifurcation, is analyzed. On the Sliding Hopf and Sliding Homoclinic bifurcations we highlight the pioneering works of Ponce and Pagano [3,4], identifying the occurrence of such bifurcations in a boost converter model, and recent studies with application in systems compose by interconnected power converters in an islanded direct current (DC) microgrid, in the works of Cristiano et al. [27] and Benadero et al. [28]. In both the analysis is partial, without delving into these subjects. Here, we will analyze them in more detail.

The main contribution of this paper is the characterization of a new mechanism to produce a homoclinic bifurcation, where the closing point of the homoclinic loop is a two-fold singularity. In this paper, a rigorous analysis of the Sliding Hopf and Sliding Homoclinic bifurcations is presented. In order to do that, a case study in power electronics is considered.

This paper is organized as follows. Previous results on Filippov theory are discussed in Section 2. The modeling of the boost converter with SMC, the analysis of the tangential singularities and the dynamics of the sliding vector field are shown in Section 3. The occurrence of Sliding Hopf and Sliding Homoclinic bifurcations are shown in Section 4.

2. Previous results

2.1. Filippov's convention

Let $A \subset \mathbb{R}^3$ be an open set and

$$\Sigma = \{(x, y, z) \in A \mid h(x, y, z) = 0\},$$

with $h(x, y, z) = z$. Clearly the *switching manifold* Σ is the separating boundary of the regions $\Sigma_+ = \{(x, y, z) \in A \mid z > 0\}$ and $\Sigma_- = \{(x, y, z) \in A \mid z < 0\}$.

We define $\mathfrak{X}^r$ the space of C^r-vector fields on A endowed with the C^r-topology with $r = \infty$ or $r \geq 1$ large enough for our purposes. Call Ω^r the space of vector fields $\mathbf{f} : A \to \mathbb{R}^3$ such that

$$\mathbf{f}(\mathbf{x}) = \begin{cases} \mathbf{f}^+(\mathbf{x}), & \text{for } \mathbf{x} \in \Sigma_+, \\ \mathbf{f}^-(\mathbf{x}), & \text{for } \mathbf{x} \in \Sigma_-, \end{cases}$$

where $\mathbf{x} = (x, y, z) \in A$, $\mathbf{f}^\pm = (f_1^\pm, f_2^\pm, f_3^\pm) \in \mathfrak{X}^r$. We may consider $\Omega^r = \mathfrak{X}^r \times \mathfrak{X}^r$ endowed with the product topology and denote any element in Ω^r by $\mathbf{f} = (\mathbf{f}^+, \mathbf{f}^-)$, which we will accept to be multivalued in points of Σ.

The kind of contact of smooth vector fields $\mathbf{f}^\pm \in \mathfrak{X}^r$ with Σ are provided by the directional Lie derivatives:

$$L_{\mathbf{f}^\pm} h = \langle \nabla h, \mathbf{f}^\pm \rangle = f_3^\pm,$$

where ∇h and $\langle ., . \rangle$ denote the gradient of smooth function h and the canonical inner product, respectively. The higher order Lie derivatives are given by $L^m_{\mathbf{f}^\pm} h = \langle \nabla L^{m-1}_{\mathbf{f}^\pm} h, \mathbf{f}^\pm \rangle$.

On Σ we distinguish the following regions:

- Crossing regions, defined by $\Sigma^{c+} = \{\mathbf{x} \in \Sigma \mid f_3^+(\mathbf{x}) > 0, f_3^-(\mathbf{x}) > 0\}$ and $\Sigma^{c-} = \{\mathbf{x} \in \Sigma \mid f_3^+(\mathbf{x}) < 0, f_3^-(\mathbf{x}) < 0\}$;
- Sliding region, defined by $\Sigma^s = \{\mathbf{x} \in \Sigma \mid f_3^+(\mathbf{x}) < 0, f_3^-(\mathbf{x}) > 0\}$;
- Escaping region, defined by $\Sigma^e = \{\mathbf{x} \in \Sigma \mid f_3^+(\mathbf{x}) > 0, f_3^-(\mathbf{x}) < 0\}$.

When $\mathbf{x} \in \Sigma^s$, following the Filippov's convention (see [2]), the *sliding vector field* associated to $\mathbf{f} \in \Omega^r$ is the vector field $\widehat{\mathbf{f}}^s$ tangent to Σ expressed in coordinates as

$$\widehat{\mathbf{f}}^s(\mathbf{x}) = \frac{1}{(f_3^- - f_3^+)(\mathbf{x})} \begin{bmatrix} (f_1^+ f_3^- - f_1^- f_3^+)(\mathbf{x}) \\ (f_2^+ f_3^- - f_2^- f_3^+)(\mathbf{x}) \\ 0 \end{bmatrix}. \tag{1}$$

Associated to (1) there exists the *planar normalized sliding vector field*

$$\mathbf{f}^s(x, y) = \begin{bmatrix} (f_1^+ f_3^- - f_1^- f_3^+)(x, y) \\ (f_2^+ f_3^- - f_2^- f_3^+)(x, y) \end{bmatrix}. \tag{2}$$

Note that, if $\mathbf{x} \in \Sigma^s$ then $f_3^+(x, y) < 0$ and $f_3^-(x, y) > 0$. So, $(f_3^- - f_3^+)(x, y) > 0$ and therefore, $\widehat{\mathbf{f}}^s$ and $\mathbf{f}^s$ are topologically equivalent in Σ^s, $\mathbf{f}^s$ has the same orientation as $\widehat{\mathbf{f}}^s$ and it can be C^r-extended to the closure $\overline{\Sigma^s}$ of Σ^s (see [5]). We can take advantage of the invariance of Σ under the flow determined by $\mathbf{f}^s$ and reduce the dimension of the problem by one, taking $z = 0$. So, all the analysis of the sliding dynamics contained in this work is based on the planar normalized sliding vector field $\mathbf{f}^s(x, y)$.

The points $\mathbf{q} \in \Sigma$ such that $\widehat{\mathbf{f}}^s(\mathbf{q}) = \mathbf{0}$ are called *pseudo-equilibria* of $\mathbf{f}$, virtual if $\mathbf{q} \in \Sigma^c$ or real if $\mathbf{q} \in \Sigma^s \cup \Sigma^e$. The points $\mathbf{p} \in \Sigma$ such that $f_3^+(\mathbf{p}) \cdot f_3^-(\mathbf{p}) = 0$ are called *tangential singularities* of $\mathbf{f}$ (i.e., the trajectory through $\mathbf{p}$ is tangent to Σ). Furthermore, a point $\mathbf{p} \in \Sigma$ is called *double tangency point* (i.e., the trajectories of both vector fields $\mathbf{f}^\pm$ through $\mathbf{p}$ are tangent to Σ) if $f_3^+(\mathbf{p}) = f_3^-(\mathbf{p}) = 0$.

Remark 1. If $\mathbf{q} = (x_q, y_q, 0) \in \Sigma^s$ is a pseudo-equilibrium point, then $\mathbf{f}^s(x_q, y_q) = \mathbf{0}$, i.e., the projection of pseudo-equilibrium on Σ is an equilibrium point of planar normalized sliding vector field $\mathbf{f}^s$. Furthermore, if (x_q, y_q) is an equilibrium node, focus or saddle, then the pseudo-equilibrium $\mathbf{q}$ is said to be a pseudo-node, pseudo-focus or pseudo-saddle, respectively.

If $\mathbf{p} = (x_p, y_p, 0)$ is a double tangency point (i.e., $f_3^-(\mathbf{p}) = f_3^+(\mathbf{p}) = 0$), then

$$\mathbf{f}^s(x_p, y_p) = \begin{bmatrix} f_1^+ f_3^-(\mathbf{p}) - f_1^- f_3^+(\mathbf{p}) \\ f_2^+ f_3^-(\mathbf{p}) - f_2^- f_3^+(\mathbf{p}) \end{bmatrix} = \begin{bmatrix} 0 \\ 0 \end{bmatrix}.$$

So, the point (x_p, y_p) is also an equilibrium of the planar sliding vector field $\mathbf{f}^s$. The interesting point here is that the sliding dynamics is not defined at (x_p, y_p). However, this point governs the sliding dynamics around it, acting as a true equilibrium point from the analysis of $\mathbf{f}^s$.

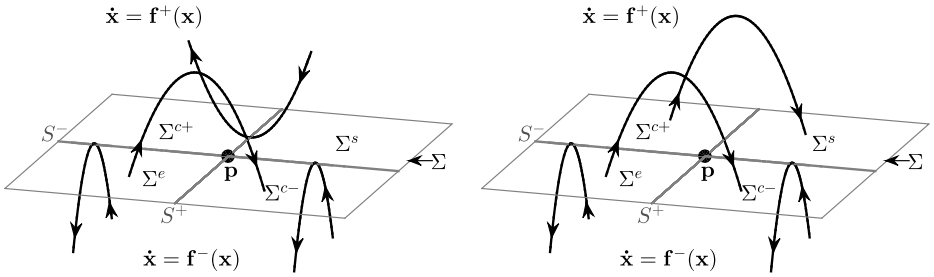

Fig. 1. On the left it appears a fold–cusp singularity and on the right a two-fold singularity, at the point **p**.

2.2. Tangential singularities

In our approach we deal with two important distinguished tangential singularities: the points where the contact between the trajectory of $\mathbf{f}^+$ or $\mathbf{f}^-$ with Σ is either quadratic or cubic, which are called *fold* and *cusp* singularities, respectively (see [29]). Observe that this contact is characterized by Lie's derivative, defined in the previous section.

A point $\mathbf{p} \in \Sigma$ is a fold point of $\mathbf{f}^+$ if $L_{\mathbf{f}^+}h(\mathbf{p}) = 0$ and $L^2_{\mathbf{f}^+}h(\mathbf{p}) \neq 0$. Moreover, $\mathbf{p}$ is a cusp point of $\mathbf{f}^+$ if $L_{\mathbf{f}^+}h(\mathbf{p}) = L^2_{\mathbf{f}^+}h(\mathbf{p}) = 0, L^3_{\mathbf{f}^+}h(\mathbf{p}) \neq 0$ and $\{dh(\mathbf{p}), d(L_{\mathbf{f}^+}h)(\mathbf{p}), d(L^2_{\mathbf{f}^+}h)(\mathbf{p})\}$ is a linearly independent set. We define the sets of tangential singularities $S^+ = \{\mathbf{p} \in \Sigma \mid f_3^+(\mathbf{p}) = 0\}$ and $S^- = \{\mathbf{p} \in \Sigma \mid f_3^-(\mathbf{p}) = 0\}$.

In $\mathbb{R}^3$, through a generic cusp singularity emanate two branches of fold singularities, see Fig. 1. In one branch it appears visible fold singularities and in the other one invisible fold singularities.

When $\mathbf{p}$ is a fold, cusp singularity of both smooth vector fields (i.e., $\mathbf{p}$ is a double tangency point) we say that $\mathbf{p}$ is a *two-fold singularity*, *two-cusp singularity*, respectively. When $\mathbf{p}$ is a fold singularity for one smooth vector field and a cusp singularity for the other one, we say that $\mathbf{p}$ is a *fold–cusp singularity*, see Fig. 1.

3. A case study in power electronics: controlling the boost converter

The behavior of a dc–dc boost converter, considering the ideal case, can be studied using the circuit topology depicted in Fig. 2. The model of the boost converter controlled by a SMC-Washout, in the continuous conduction mode, is given by

$$L\frac{di_L}{dt} = V_{in} - u\, v_C \tag{3}$$

$$C\frac{dv_C}{dt} = u\, i_L - \frac{v_C}{R} \tag{4}$$

$$\frac{dz_F}{dt} = \omega_F(i_L - z_F), \tag{5}$$

where $v_C \geq 0$ and $i_L > 0$ are the instantaneous capacitor voltage and the inductor current, respectively. The input voltage is assigned as V_{in}, R is the equivalent load resistance, C and L are the circuit capacitor and inductor, respectively. The inductor current i_L passes through a washout filter and a new variable z_F is obtained by (5), whereas the cut-off frequency of the filter is denoted by ω_F and always less than $1/\sqrt{LC}$ rad/s that is the approximate natural frequency of the system (see [30]).

The control law is defined as $u = \frac{1}{2}(1+\text{sign}[h])$ such that $u = 1$ implies that the switch S, in Fig. 2, is off and $u = 0$ corresponds to the switch S on. The planar switching surface is chosen as

$$h(i_L, v_C, z_F) = v_C - V_{ref} + K(i_L - z_F) = 0,$$

where $K > 0$ is the control parameter to be adequately tuned and $V_{ref} > V_{in}$ is the reference voltage since the control goal is to regulate the voltage output $v_0 = v_C$ of the boost converter, being $v_0 > V_{in}$.

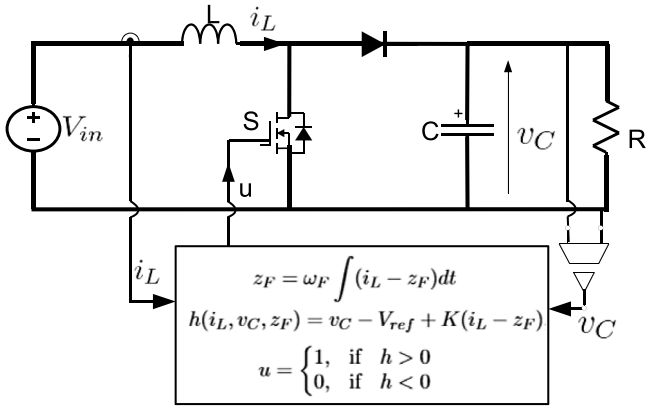

Fig. 2. Boost converter with SMC-washout.

Eqs. (3)–(5) can be normalized by applying the following change of variables: $i_L = V_{in}\sqrt{\frac{C}{L}}x$, $v_C = V_{in}y$, $z_F = i_L + \frac{v_C - V_{ref} - V_{in}z}{K}$; and time $t = \sqrt{LC}\tau$. Defining the new parameters: $a = \frac{1}{R}\sqrt{\frac{L}{C}}$, $k = K\sqrt{\frac{C}{L}}$, $\omega = \omega_F\sqrt{LC}$ and $y_r = \frac{V_{ref}}{V_{in}}$, the dimensionless model is given by

$$\begin{aligned} \dot{x} &= 1 - uy \\ \dot{y} &= ux - ay \\ \dot{z} &= u(x - ky) + (\omega - a)y - \omega z + k - \omega y_r, \end{aligned} \tag{6}$$

where $(x, y, z) \in D \subset \mathbb{R}^3$ are the independent variables and the parameters are $\omega \in (0, 1]$, $y_r > 1$, $k > 0$ and $a > 0$ (the dot "$\cdot$" indicates $\frac{d}{d\tau}$). We stress that $x > 0$ is the normalized inductor current, $y \geq 0$ is the normalized output voltage and $z \in \mathbb{R}$ depends on the filtered current.

For the normalized system (6), redefined the planar switching surface as $h_n(x, y, z) = h(i_L, v_C, z_F)/V_{in} = z = 0$, the control rewritten as

$$u = \frac{1}{2}(1 + \text{sign}[z]) \tag{7}$$

and the switching manifold as $\Sigma = \{(x, y, z) \in \mathbb{R}^3 : z = 0\}$. System (6) with the control law (7) can be represented by a piecewise smooth dynamical system $(\dot{x}, \dot{y}, \dot{z}) = \mathbf{f}(x, y, z)$ with

$$\mathbf{f}(\mathbf{x}) = \begin{cases} \mathbf{f}^+ = (1 - y, x - ay, f_3^+) & \text{if } z > 0 \\ \mathbf{f}^- = (1, -ay, f_3^-) & \text{if } z < 0, \end{cases} \tag{8}$$

where $\mathbf{x} = (x, y, z)$ and

$$f_3^+(x, y, z) = x + (\omega - a - k)y - \omega z + k - \omega y_r,$$

$$f_3^-(x, y, z) = (\omega - a)y - \omega z + k - \omega y_r.$$

Remark 2. In the sequel we consider $0 < a < 2$. This is a coherent physical hypothesis and it is enough to produce the desired behavior.

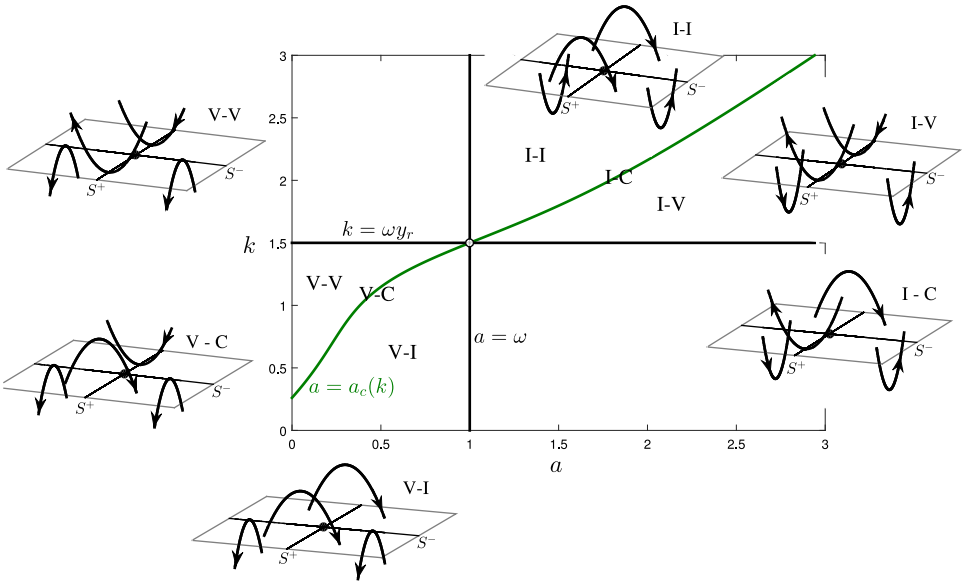

Fig. 3. Kinds of the double tangency point in the (a, k)-plane, according to Table 1. The quadrants $\{k > \omega y_r\} \cap \{a < \omega\}$ and $\{k < \omega y_r\} \cap \{a > \omega\}$ are not considered in our study according to Remark 3.

3.1. Tangential singularities

The tangential sets of $\mathbf{f}^+$ and $\mathbf{f}^-$ are given, respectively, by the *straight lines*:

$$S^+ = \{(x, y, 0) \in \Sigma : x = (a + k - \omega)y - k + \omega y_r\},$$
$$S^- = \left\{(x, y, 0) \in \Sigma : y = \frac{k - \omega y_r}{a - \omega}, \text{ for } a \neq \omega\right\}.$$

The next result summarizes the possibilities of tangential singularities according to the parameters a, y_r, k and ω.

A straightforward calculation shows that the point $\mathbf{p}_c = (x_c, y_c, 0)$ with

$$x_c = \frac{\omega(y_r - 1) + a(1 + (a + k - \omega)(k - \omega y_r))}{(a + k - \omega)(k - \omega) + 1}$$
$$y_c = \frac{(a + k - \omega)(k - \omega y_r) + 1}{(a + k - \omega)(k - \omega) + 1},$$

is a *cusp singularity*, since $L^2_{\mathbf{f}^+} h(\mathbf{p}_c) = 0$ and the third Lie derivative evaluated at the cusp point is given by $L^3_{\mathbf{f}^+} h(\mathbf{p}_c) = \omega(1 - y_r) < 0$, i.e., the trajectory of $\mathbf{f}^+$ passing through the cusp point $\mathbf{p}_c$ departs from Σ. The point $\mathbf{p}_c$ separates S^+ into two branches of fold singularities. The *branch of visible fold singularities* for $y < y_c$ and the *branch of invisible fold singularities* for $y > y_c$.

Since $L^2_{\mathbf{f}^-} h(\mathbf{p}) = a(k - \omega y_r)$ for all $\mathbf{p} \in S^-$ we get that all points in S^- are *invisible fold singularities* if $k > \omega y_r$, or *visible fold singularities* if $k < \omega y_r$.

The double tangency point, $\mathbf{p}_t$, is given by $S^+ \cap S^-$, i.e.,

$$\mathbf{p}_t = \left(\frac{k(k - y_r\omega)}{a - \omega}, \frac{k - \omega y_r}{a - \omega}, 0\right). \tag{9}$$

The point $\mathbf{p}_t$ is a two-fold singularity if $a \neq a_c(k)$ or a fold–cusp singularity if $a = a_c(k)$, for all $k \neq \omega y_r$, where

$$a_c(k) = \frac{1}{2(k - \omega y_r)}\Big[-1 + \omega(k - \omega y_r) + \sqrt{1 + (k - \omega y_r)(2\omega + (4 + (\omega - 2k)^2)(k - \omega y_r))}\Big]. \tag{10}$$

Table 1
Kinds of tangential points according to the parameters (a, k).

Kind of tangency (legend)	Region on the plane (a, k)
Two-Fold Visible–Invisible (V–I)	$a_c(k) < a < \omega$ for $k < \omega y_r$
Two-Fold Visible–Visible (V–V)	$a < a_c(k)$ for $k < \omega y_r$
Two-Fold Invisible–Invisible (I–I)	$\omega < a < a_c(k)$ for $k > \omega y_r$
Two-Fold Invisible–Visible (I–V)	$a > a_c(k)$ for $k > \omega y_r$
Fold Invisible–Cusp (I–C)	$a = a_c(k)$ for $k > \omega y_r$
Fold Visible–Cusp (V–C)	$a = a_c(k)$ for $k < \omega y_r$

Table 1 shows the kinds of double tangency points according to the parameters (a, k). Following, choosing $\omega = 1$ and $y_r = 3/2$, we represent Table 1 in the plane of parameters (a, k) shown in Fig. 3. Taking a point (a, k) in one of the regions V–I, V–V, I–V or I–I, we obtain a double tangency fold of the type visible–invisible, visible–visible, invisible–visible or invisible–invisible, respectively. While, for points (a, k) on the curve $a = a_c(k)$ the double tangency is of the kind fold (invisible in part I–C or visible in part V–C) on one side and cusp on the other. For each one of the kinds cited, we illustrate (on the side) the geometry involving the "invisible" and "visible" dynamics of the vector fields $\mathbf{f}^+$ and $\mathbf{f}^-$ around the double tangency point.[1]

Remark 3. Observe that, for practical reasons, $x > 0$ and $y > 0$. As consequence, in $\mathbf{p}_t$, either $a > \omega$ and $k > \omega y_r$ or $a < \omega$ and $k < \omega y_r$.

3.2. Dynamics of the sliding vector field

The sliding vector field is calculated from Eq. (1), resulting in

$$\widehat{\mathbf{f}}^s(\mathbf{x}) = \frac{1}{x - ky}\begin{bmatrix} x - ay^2 + \omega y(y - y_r - z) \\ -k(x - ay^2) - \omega x(y - yr - z) \\ 0 \end{bmatrix}, \tag{11}$$

[1] In the expressions Visible–Invisible, Visible–Visible, Invisible–Visible, Invisible–Invisible, Fold Invisible–Cusp and Fold Visible–Cusp, the first description refers to the vector field $\mathbf{f}^-$ and the second to the vector field $\mathbf{f}^+$. For example, Visible–Invisible indicates a two-fold whose quadratic tangency is visible to $\mathbf{f}^-$ and invisible to $\mathbf{f}^+$, or even, Fold Invisible–Cusp, where the double tangency is quadratic invisible to $\mathbf{f}^-$ and cubic to $\mathbf{f}^+$.

whose equilibrium point is

$$\mathbf{q} = (ay_r^2, y_r, 0). \tag{12}$$

This is the operating point of the boost converter controlled by the proposed SMC-Washout. The washout filter is responsible for the elimination of the output voltage dependence in relation to the changes of the parameter a produced by load changes of R. In this way, after a perturbation on a, the output voltage maintains the desired value y_r.

Now, we proceed to analyze the parameter conditions to obtain a pseudo-equilibrium $\mathbf{q}$ real and located in the sliding region. In order to do that, the following conditions

$$L_{\mathbf{f}^-}h(\mathbf{q}) = k - ay_r > 0,$$
$$L_{\mathbf{f}^+}h(\mathbf{q}) = -(y_r - 1)(k - ay_r) < 0,$$

must be verified such that $\mathbf{q} \in \Sigma^s$. We remember that the parameter $y_r > 1$. Therefore, if $k - ay_r > 0$ (respectively, $k - ay_r < 0$) then $\mathbf{q} \in \Sigma^s$ (respectively, $\mathbf{q} \in \Sigma^e$) and if $k - ay_r = 0$ then $\mathbf{q}$ coincides with the double tangency point $\mathbf{p}_t$ given in (9).

In the sliding mode control it is necessary that the pseudo-equilibrium (i.e., the operating point) remains in the sliding region Σ^s. So, the control parameter k must fulfill:

$$k > ay_r. \tag{13}$$

Moreover, the pseudo-equilibrium must be stable and whenever possible, without to exhibit an unstable limit cycle around it in order to enlarge the stability region.

In order to analyze the stability of the pseudo-equilibrium $\mathbf{q}$, we use the sliding vector field $\mathbf{f}^s$ calculated from (2), given by

$$\mathbf{f}^s(x, y) = \begin{bmatrix} -x + ay^2 - \omega y(y - y_r) \\ k(x - ay^2) + \omega x(y - yr) \end{bmatrix}. \tag{14}$$

The projection of the pseudo-equilibrium $\mathbf{q}$ in the switching manifold Σ is the point $\mathbf{q}_s = (ay_r^2, y_r)$. This point is an equilibrium of $\mathbf{f}^s$ and its stability can be extended to the pseudo-equilibrium $\mathbf{q}$ since it satisfies the condition (13).

The Jacobian matrix of the normalized sliding vector field (14) evaluated at the point $\mathbf{q}_s$ is given by

$$J(\mathbf{q}_s) = \begin{pmatrix} -1 & (2a - \omega)y_r \\ k & ay_r(\omega y_r - 2k) \end{pmatrix}.$$

The determinant and trace of $J(\mathbf{q}_s)$, are given by

$$\mathrm{Det}[J(\mathbf{q}_s)] = \omega y_r(k - ay_r),$$
$$\mathrm{Tr}[J(\mathbf{q}_s)] = -1 + ay_r(\omega y_r - 2k).$$

Imposing the condition (13) on the parameter k, then $\mathrm{Det}[J(\mathbf{q}_s)] > 0$. Therefore, the pseudo-equilibrium $\mathbf{q}$, when in Σ^s, can be a pseudo-node or pseudo-focus, stable or unstable. In this case it will be stable if and only if, $\mathrm{Tr}[J(\mathbf{q}_s)] < 0$, i.e., k must be chosen such that it fulfills, in addition of (13), inequality

$$k > \frac{a\omega y_r^2 - 1}{2ay_r}. \tag{15}$$

Remark 4. If $k < ay_r$ the pseudo-equilibrium $\mathbf{q}$ is on the escaping region Σ^e and it is a pseudo-saddle, because $\mathrm{Det}[J^e(\mathbf{q}_s)] = \mathrm{Det}[J(\mathbf{q}_s)] < 0$, where J^e is the Jacobian matrix of the normalized sliding vector field defined on Σ^e as $\mathbf{f}^e(x, y) = -\mathbf{f}^s(x, y)$.

More precisely, in order to distinguish if $\mathbf{q}$ is a pseudo-focus or a pseudo-node we have to analyze the sign of the discriminant Δ of the characteristic polynomial of $J(\mathbf{q}_s)$. Explicitly,

$$\Delta = \mathrm{Tr}[J(\mathbf{q}_s)]^2 - 4\mathrm{Det}[J(\mathbf{q}_s)]$$
$$= 4a^2y_r^2k^2 - 4y_r(\omega + a(a\omega y_r^2 - 1))k + (1 + a\omega y_r^2)^2.$$

Table 2
Kinds of dynamics of the sliding vector field at pseudo-equilibrium point $\mathbf{q}$, according to parameters (a, k).

Kind of dynamics	Conditions under the parameters (a, k)
Pseudo-saddle	$k < ay_r$
Stable pseudo-node	$k > ay_r$ and $a \geq \frac{\omega}{2}$, or $k > k_+$ and $a < \frac{\omega}{2}$, or $ay_r < k < k_-$ and $a_+ < a < \frac{\omega}{2} \cup 0 < a < a_-$
Unstable pseudo-node	$ay_r < k < k_-$ and $a_- < a < a_+$
Stable pseudo-focus	$k_- < k < k_+$ and $a_+ < a < \frac{\omega}{2} \cup 0 < a < a_-$, or $k_H < k < k_+$ and $a_- < a < a_+$
Unstable pseudo-focus	$k_- < k < k_H$ and $a_- < a < a_+$

This expression is a polynomial of degree two in the variable k. The solutions of $\Delta = 0$ are given by:

$$k_\pm = k_H + \frac{\omega \pm \sqrt{\omega(1 + 2a^2y_r^2)(\omega - 2a)}}{2a^2y_r}, \tag{16}$$

where

$$k_H = \frac{a\omega y_r^2 - 1}{2ay_r}. \tag{17}$$

Note that $k > k_H$ satisfies the stability condition (15) and $k = k_H$ implies $\mathrm{Tr}[J(\mathbf{q}_s)] = 0$. Furthermore, the roots $k_\pm$ of polynomial $\Delta = 0$ exist only for $a \leq \frac{\omega}{2}$, otherwise we will have $\Delta > 0$ for all k.

In Table 2, we summarize these results on the dynamics of the sliding vector field at the pseudo-equilibrium point $\mathbf{q}$. These stability conditions were obtained considering that $y_r \geq \frac{2\sqrt{2}}{\omega}$, otherwise $\mathbf{q}$ is always stable for all $k > ay_r$. This condition on the parameter y_r assures us the existence of a *Bogdanov–Takens* bifurcation (BT) at points $(a_-, y_r a_-)$ and $(a_+, y_r a_+)$ of the (a, k)-plane (see Fig. 8), such that

$$a_\pm = \frac{1}{4y_r}\left(\omega y_r \pm \sqrt{\omega^2 y_r^2 - 8}\right). \tag{18}$$

The Hopf and Homoclinic bifurcations corresponding to the sliding vector field of the boost converter system with SMC-Washout are studied in the next section.

4. A sliding Hopf bifurcation followed by a homoclinic loop at the two-fold singularity

In this section we analyze two bifurcations that occur in the sliding vector field (11). First a Sliding Hopf bifurcation takes place giving rise to a unstable limit cycle C. Second, C persists when the parameter k varies (from $k = 1.375$ to $k = 1.573$, for the case $\omega = 1$, $y_r = 4$, $a = 0.2$, see simulations in Figs. 4–5 and the bifurcation diagrams in Fig. 6), and then it collides with the two-fold point, which behaves like a saddle. This collision produces a homoclinic loop destroying the limit cycle.

4.1. Sliding Hopf bifurcation

In previous section, we proved that $\mathbf{q}$ is an unstable focus when $k_- < k < k_H$ and a stable one when $k_H < k < k_+$, since $a_- < a < a_+$. Then we can state the following result:

Proposition 1. *If $k = k_H$ and $a \in (a_-, a_+)$, where $a_\pm$ are given in (18) and k_H is given in (17), then a subcritical Hopf bifurcation occurs at $\mathbf{q} = (ay_r^2, y_r, 0)$ in the sliding vector field (11).*

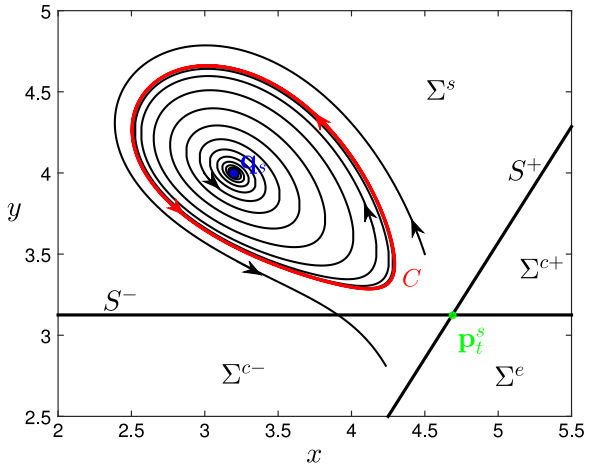

(a) Projection on Σ.

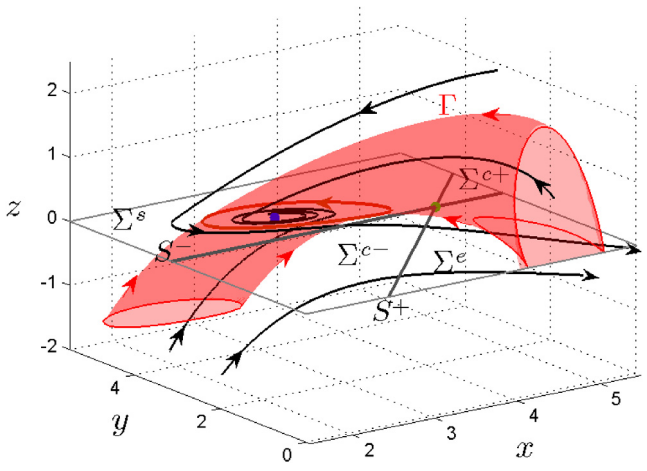

(b) Three-dimensional basin of attraction of the pseudo-equilibrium point displayed in red color.

Fig. 4. Unstable limit cycle in the nonsmooth vector field (8) and the corresponding basin of attraction for $\omega = 1, y_r = 4, a = 0.2$ and $k = 1.5$. (For interpretation of the references to color in this figure legend, the reader is referred to the web version of this article.)

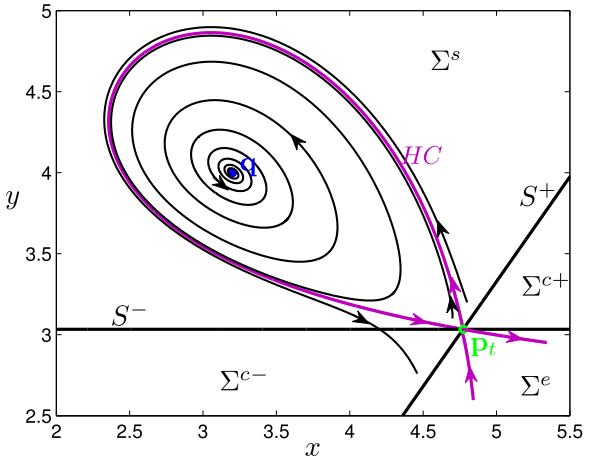

(a) Projection on Σ.

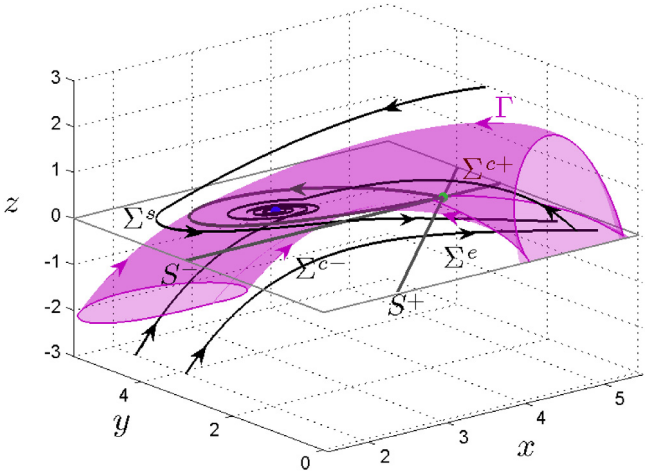

(b) Three-dimensional basin of attraction of the pseudo-equilibrium point displayed in purple color.

Fig. 5. Homoclinic loop at the two-fold point and the corresponding basin of attraction for $\omega = 1, y_r = 4, a = 0.2$ and $k = 1.573$. (For interpretation of the references to color in this figure legend, the reader is referred to the web version of this article.)

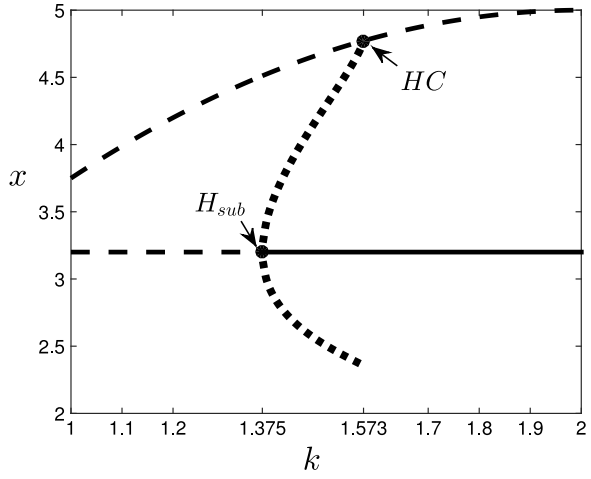

(a) (x, k)-plane.

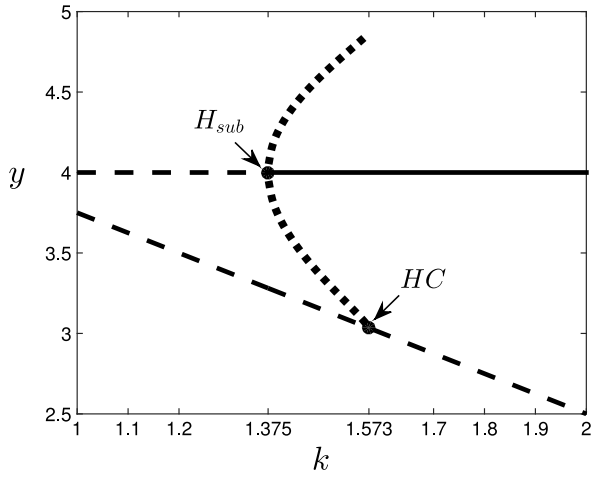

(b) (y, k)-plane.

Fig. 6. Bifurcation diagrams showing the Hopf and Homoclinic sliding bifurcations in (x, k)-plane and (y, k)-plane, considering k as the bifurcation parameter, for $\omega = 1$, $y_r = 4, a = 0.2$. The dashed and solid lines represent unstable and stable equilibria, respectively. While the dotted line represents the unstable limit cycle.

Proof. For this proof, we consider the planar sliding vector field (14) that is topologically equivalent to (11) in Σ^s and the projection of pseudo-equilibrium $\mathbf{q}$ in Σ given by $\mathbf{q}_s = (ay_r^2, y_r)$.

The following necessary conditions to get a Hopf bifurcation are satisfied for $k = k_H$:

$$\left.\mathrm{Det}[J(\mathbf{q}_s)]\right|_{k=k_H} = \frac{\omega(-1+\omega y_r^2 a - 2y_r^2 a^2)}{2a} > 0$$

$$\left.\mathrm{Tr}[J(\mathbf{q}_s)]\right|_{k=k_H} = 0$$

$$\left.\frac{d\mathrm{Tr}[J(\mathbf{q}_s)]}{dk}\right|_{k=k_H} = -2ay_r \neq 0,$$

since $a_- < a < a_+$. Then let us consider the system

$$\begin{aligned} \dot{u} &= u + v(\omega(v + y_r) - a(v + 2y_r)) \\ \dot{v} &= -v\omega(u + ay_r^2) + k(-u + av(v + 2y_r)), \end{aligned} \tag{19}$$

obtained from a translation of (14) in such a way that $\mathbf{q}_s$ is translated to the origin.

According to [14] (see page 253), if the number

$$\sigma = -\frac{1}{y_r(2a-\omega)\sqrt{\frac{\omega^3(ay_r^2(\omega-2a)-1)^3}{a^3}}}(3\sqrt{2}\pi\omega(-2a^2k^2y_r + a(2k^3 + k^2\omega y_r + k - 2\omega y_r) + \omega(k + \omega y_r)))$$

is not null, then a Hopf bifurcation occurs at the origin in the planar analytic system (19). In fact, the number σ, also known as *Lyapunov coefficient*, is the first non null coefficient of the Taylor's polynomial expansion of the displacement map $d(x) = \varphi(x) - x$, where $\varphi(x)$ is the first return map associated to (19) (see [18] for details). Moreover, we have $\sigma > 0$ for all $a \in (a_-, a_+)$ and, thus, a subcritical Hopf bifurcation occurs when $k = k_H$. Therefore, a unique unstable limit cycle bifurcates from the point $\mathbf{q}$ in the sliding vector field (11) (see Fig. 4(a)–(b)). So Proposition 1 is proved. □

Fig. 4(a) and (b) show the phase portrait of (14) and a simulation of the behavior of the boost converter with the SMC-Washout given by (8), respectively. On both we note the existence of an unstable limit cycle $C \subset \Sigma^s$ around the stable focus $\mathbf{q} \in \Sigma^s$. The red closed curve, the blue point and the green point represent the limit cycle C, the pseudo-equilibrium point $\mathbf{q}$ and the two-fold point $\mathbf{p}_t$, respectively. While the red solid denoted by Γ indicates the basin of attraction of the pseudo-equilibrium $\mathbf{q}$ (more details in Section 4.3). The parameter values used in the simulation are: $\omega = 1, y_r = 4, a = 0.2$ and $k = 1.5$.

4.2. Sliding homoclinic bifurcation

The unique limit cycle C, that emerged from the Sliding Hopf Bifurcation of Section 4.1, persists until the homoclinic loop occurs at the two-fold point. This is the subject of the next proposition.

Proposition 2. *The limit cycle C emerges from the Sliding Hopf Bifurcation in Proposition 1, when the parameter k assumes the critical value $k = k_H$. It persists when the parameter k varies from $k = k_H$ to $k = k_{HC}$, where k_{HC} stands for the critical value of parameter k needed to connect the limit cycle with the two-fold point, until to touch the homoclinic loop at the two-fold point and then disappears.*

Proof. According to Table 1, the double tangency point $\mathbf{p}_t$ is a visible–invisible two-fold singularity whenever $a_c(k) < a < \omega$ and $k < \omega y_r$. Note that the sliding Homoclinic bifurcation curve in plane $-(a, k)$ is contained in the quadrant $a_- < a < a_+$ and $y_r a_- < k < y_r a_+$ (see Fig. 8). As $a_+ < \frac{\omega}{2}$ and $a_- > a_c$, then the double tangency point is classified as visible–invisible two-fold when the sliding Homoclinic bifurcation occurs.

Moreover, the projection of the point $\mathbf{p}_t$ on the switching manifold Σ is the point $\mathbf{p}_t^s = (ky_t, y_t)$, where $y_t > 0$ is the coordinate y of the double tangency point $\mathbf{p}_t$ given in (9). The point $\mathbf{p}_t^s$ is an equilibrium of the planar normalized sliding vector field $\mathbf{f}^s$, whose dynamics in its neighborhood on Σ^s is saddle type whenever the $\mathbf{q} \in \Sigma^s$, because

$$\mathrm{Det}[J(\mathbf{p}_t^s)] = -\omega(k - ay_r)y_t < 0$$

for $k > ay_r$. Thus it is natural that the homoclinic loop passes through this point.

Since the two coordinates of system (14) have no roots in common and the cycle emerged from Proposition 1 is unique, we are able to use the *Perko's Planar Termination Principle* (see [31,32]). More precisely, the parameter k represents the Hopf bifurcation parameter and this principle guarantees that this family of periodic orbits is unbounded or terminates at a critical point as shown in Fig. 5(a). So, we conclude that the family of periodic orbits persists until reach a saddle point defined by the separatrices of $\mathbf{p}_t^s$, which is a visible–invisible two-fold point, giving rise to a homoclinic loop. See Fig. 5(a)–(b). □

The previous proposition states the existence of homoclinic bifurcation for the normalized sliding vector fields $\mathbf{f}^s$. Note that this vector field is smooth and therefore the homoclinic orbit possesses the two-fold point $\mathbf{p}_t^s$ as α- and ω-limits, which is reached when $t \to -\infty$ and $t \to +\infty$, respectively. However, the trajectories of the vector fields f^+ and f^- reach the two-fold point in a finite time. This is an important issue and a difference between the smooth and piecewise smooth world.

Fig. 5(a) and (b) illustrate the phase portrait of (14) and the simulations of the boost converter with SMC-Washout given by (8), respectively. In Fig. 5(a) we observe the homoclinic loop (purple curve) passing through $\mathbf{p}_t^s$ (projection of $\mathbf{p}_t$ in Σ) that is a saddle equilibrium point of $\mathbf{f}^s$ and is the closing point of the homoclinic orbit. In Fig. 5(b), the purple solid represents the basin of attraction Γ of the pseudo-equilibrium $\mathbf{q}$; and $\mathbf{p}_t$ (green dot) is a visible–invisible two-fold singularity of the model. The parameter values used in the simulation are: $\omega = 1, y_r = 4, a = 0.2$ and $k = 1.573$.

Remark 5. The homoclinic loop L_0 is simple since

$$\sigma_0 = \nabla \cdot \mathbf{f}^s = \mathrm{Tr}[J(\mathbf{p}_t^s)] = \frac{k(2a-\omega)(\omega y_r - k)}{a - \omega} - 1 \neq 0.$$

We say that a separatrix cycle is called stable or unstable if the displacement map $d(s)$ satisfies $d(s) < 0$ or $d(s) > 0$, respectively, for all s in some neighborhood of $s = 0$ where $d(s)$ is defined.

As shown in [14] (see page 304), if L_0 is simple ($\sigma_0 \neq 0$), the homoclinic loop L_0 is stable (unstable) if and only if $\sigma_0 < 0$ ($\sigma_0 > 0$) and besides that there exists some neighborhoods V_ε of L_0 and $\mathcal{V}$ of $\mathbf{f}^s$ (in a C^1-norm) such that for all vector field $g \in \mathcal{V}$ has at most one limit cycle in V_ε with the same stability of L_0. Moreover, as expected, from this homoclinic loop can arise from a homoclinic bifurcation only one limit cycle, as proved in [14] (see page 309).

4.3. A brief comment about the basin of attraction

An important part of the local stability analysis is the determination of the *basin of attraction* (see [33]), because it reveals the region in the state space where for any initial condition the system (8) reaches its equilibrium point. The basin of attraction, here, is defined as the subset of $\mathbb{R}^3$ formed by all the initial states $\mathbf{x}_0 = \mathbf{x}(\tau_0)$, $\tau_0 \geq 0$, that reach the switching boundary Σ on the sliding region Σ^s (in finite time $\tau = \tau_1 \geq \tau_0$), and remain confined

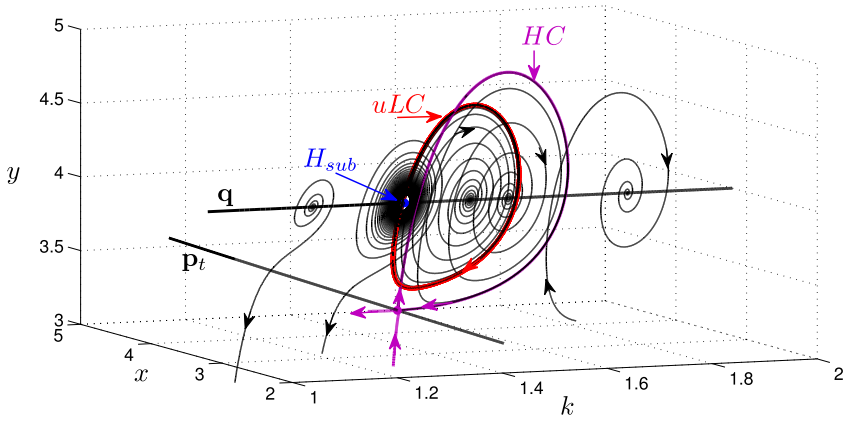

Fig. 7. Bifurcation diagram in (x, y, k)-space considering k as the bifurcation parameter. The "uLC" stands for unstable limit cycle.

to Σ (for all positive time $\tau > \tau_1$) sliding under the dynamics of $\mathbf{f}^s$, tending asymptotically to the pseudo-equilibrium $\mathbf{q} = \mathbf{x}(\infty)$.

The knowledge of the basin of attraction for different values of the control parameter k is of great importance for the control design, because it allows us to find a value for k in which the basin of attraction of the pseudo-equilibrium is maximum. However, the complete analysis of the attraction basin is a difficult task and in general is not analytically solvable. This is a very comprehensive topic and we leave the complete analysis out of this work. What we will do next in this subsection is a previous analysis on the subject from the results obtained with the analysis of the sliding Hopf and sliding Homoclinic bifurcations present in the previous subsections.

We present the case shown in Fig. 4(b), where the presence of a limit cycle $C \in \Sigma^s$ creates a solid Γ with cylindrical shape representing the basin of attraction. In this case, the boundary of the basin of attraction is formed by all initial states that reach Σ^s exactly on the unstable limit cycle C. Note that our set of initial states for the boost converter to reach the operating point is reduced to the interior of the solid Γ.

The area in Σ^s delimited by the unstable limit cycle around the stable pseudo-focus, represents the basin of attraction confined to Σ^s. We have seen in the previous subsections that this area persists with the increase in the value of parameter k (for a fixed value of a). The basin of attraction in Σ^s becomes larger when we increase the value of k. This increase can be observed by comparing Figs. 4(a) and 5(a), and also, numerically verified from the bifurcation diagrams in Fig. 6, which indicate an amplitude of limit cycle C, in both state variables, increasing as a function of k. These arguments lead us to a basin of attraction in $\mathbb{R}^3$ which increases along with k, as seen of Figs. 4(b) to 5(b), where the solids denoted by Γ represent the basin of attraction in each case.

From this previous analysis, it is clear that the basin of attraction containing the largest possible part of $\mathbb{R}^3$ will be obtained for some value of k after the sliding Homoclinic bifurcation and the disappearance of the unstable limit cycle C. However, further studies are needed to find the optimal value of k that maximizes the attraction domain, so we leave this task for a future work.

4.4. Final remarks

The bifurcation diagrams of Fig. 6 show the displacement in the x and y coordinates of the points of pseudo-equilibrium and double tangency and the variation of amplitude of the limit cycle C as a function of the parameter k. These numerical results are expected according to the analysis of bifurcations discussed in the previous subsections, where we prove that, by varying parameter k in an increasing way, the system (8) undergoes a subcritical sliding Hopf bifurcation followed by a sliding Homoclinic bifurcation. Moreover, we verified through the analysis of the bifurcation diagrams that the amplitude of C is an increasing function of k, starting (with zero amplitude) in the Hopf and disappearing (with maximum amplitude) in the Homoclinic.

In Fig. 6 is shown: the dotted curve representing the amplitude of the unstable limit cycle C; the straight line representing the coordinates x and y of $\mathbf{q}$, which is an unstable focus in the dashed part and a stable one at the solid part; the dashed curve represents the coordinates x and y of the two-fold singularity $\mathbf{p}_t$, which has characteristics of a saddle (unstable) equilibrium in the vector field sliding; the black points indicate the subcritical sliding Hopf bifurcation (H_{sub}), where the unstable limit cycle born; and the sliding Homoclinic bifurcation (HC), where the unstable limit cycle collides with the two-fold singularity $\mathbf{p}_t$ and disappears.

Fig. 7 illustrates the displacement of the pseudo-focus $\mathbf{q}$, of the two-fold singularity $\mathbf{p}_t$ and of the unstable limit cycle, in relation to the parameter k. The pseudo-focus $\mathbf{q}$ is unstable before the subcritical sliding Hopf bifurcation (H_{sub}) and stable after it. The unstable limit cycle surrounds $\mathbf{q}$ and there exists for $k \in (1.375, 1.573)$. It disappears, for $k = 1.573$, colliding to $\mathbf{p}_t$ in a homoclinic loop (HC).

We summarize the dynamics on the diagram of Fig. 8, where it can be observed that: the two points denoted as BT, given by $(a_-, y_r a_-)$ and $(a_+, y_r a_+)$ with $a_\pm$ given in (18), represent two Bogdanov–Takens bifurcations of $\mathbf{q}$; the blue curve, given by $k = k_H(a)$ with k_H defined in (17), stands for the subcritical sliding Hopf bifurcation (H_{sub}) of $\mathbf{q}$; the red curve, of equation $k = ay_r$, indicates the transcritical bifurcation (T) involving the two-fold singularity $\mathbf{p}_t$ and the pseudo-equilibrium $\mathbf{q}$; the purple curve, numerically obtained, represents the sliding Homoclinic bifurcation (HC) of C; and the green curve point out the transition of the pseudo-equilibrium $\mathbf{q}$ from node to focus.

A given value of the parameter pair (a, k) on region 1 means that $\mathbf{q}$ is a pseudo-saddle, on region 2 stands for an unstable pseudo-node, on region 3 means that it is an unstable pseudo-focus, on region 4 implies that it is a stable pseudo-node and on regions 5 and 6 denotes that it is a stable pseudo-focus (on region 5 there exists an unstable limit cycle). Moreover, on region 1 we get $\mathbf{q} \in \Sigma^e$ and on regions 2, 3, 4, 5 and 6 we get $\mathbf{q} \in \Sigma^s$.

The results obtained in this work on Sliding Hopf and Sliding Homoclinic bifurcations can be used in the control design of a boost converter. More specifically, our analysis can be used to find the values (a, k) that make the operating point locally stable, and from this, to choose the "better" value of k from a prior knowledge of the variation range of the load parameter a. Following our analysis, the

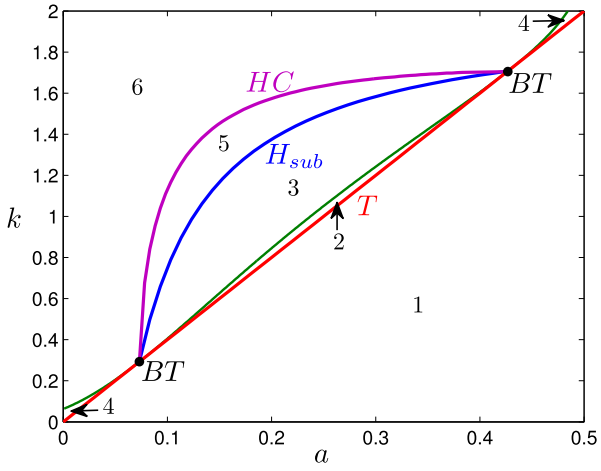

Fig. 8. Bifurcation set in (a, k)-plane.

value searched for k must be in region 6 of Fig. 8, namely the *safe operating region* of the system (8).

5. Conclusion

In this paper, by means of a case study in power electronics (boost converter controlled by a sliding mode control), we proved the existence of two different sliding bifurcations: (i) Sliding Hopf and (ii) Sliding Homoclinic. The Sliding Hopf bifurcation occurs in the sliding vector field and is analogous to the standard case. The limit cycle that arises from the Sliding Hopf bifurcation is unstable and it is confined to the switching manifold. The Sliding Homoclinic bifurcation occurs when the limit cycle disappears by touching visible–invisible two-fold point, whose dynamics in the sliding region is of the saddle type. The homoclinic loop has a sliding segment which itself closes at the two-fold singularity.

The result of the bifurcation analysis was summarized in the (a, k)-plane bifurcation set shown in Fig. 8. This methodology is useful to choose an appropriate value for the control parameter k in order to ensure the system stability at the desired operating point and prevent the birth of a limit cycle around it, even after a change in the load parameter a.

The mechanism described in the case studied in this work, from which a sliding limit cycle collapses when it touches a two-fold point is a dynamic phenomenon that is specific to nonsmooth dynamical systems. Further studies will be conducted in order to prove and to characterize this collapse mechanism for general nonsmooth dynamical systems in $\mathbb{R}^3$.

Acknowledgments

Authors are indebted to the anonymous referee for the valuable comments that allowed them to improve a previous version of the manuscript. The first author is supported by CAPES-Brazil. The second author is partially supported by grant 2014/02134-7, São Paulo Research Foundation (FAPESP), the CAPES-Brazil Grant Number 88881.030454/2013-01 from the program CSF-PVE and the CAPES Grant Number 1576689 from the program PNPD. The third author is supported by FAPEG-BRAZIL grant 2012/10 26 7000 803 and PROCAD/CAPES grant 88881.0 684 62/2014-01. The fourth author is supported by CNPq/Brazil under grant PDE-201256/2015-0. The second and third authors are supported by CNPq-BRAZIL grant 478230/2013-3 and all authors are supported by CNPq-BRAZIL grant 443302/2014-6. This work is partially realized at UFG as a part of project numbers 35796, 35797 and 040393.

References

[1] M. di Bernardo, C.J. Budd, A.R. Champneys, P. Kowalczyk, Piecewise-Smooth Dynamical Systems — Theory and Applications, Springer-Verlag, 2008.
[2] A.F. Filippov, Differential Equations with Discontinuous Righthand Sides, in: Mathematics and its Applications (Soviet Series), Kluwer Academic Publishers, Dordrecht, 1988.
[3] E. Ponce, D.J. Pagano, Sliding dynamics bifurcations in the control of boost converters. in: 18th IFAC World Congress, Milano (Italy) August 28–September 2, 2011, pp. 13293–13298.
[4] D.J. Pagano, E. Ponce, On the robustness of the DC-DC boost converter under washout SMC, in: Power Electronics Conference, Brazil, November 2009.
[5] D.J. Pagano, E. Ponce, Sliding mode controllers design through bifurcation analysis, in: Preprints 8th IFAC Symposium on Nonlinear Control Systems, Bologna, Italy, September 1–3, 2010, pp. 1284–1289.
[6] M. Castilla, L.C. de Vicuna, M. Lopez, O. Lopez, J. Matas, On the design of sliding mode control schemes for quantum resonant converters, IEEE Trans. Power Electron. 15 (2000) 960–973.
[7] Siew-Chong Tan, Y.M. Lai, Chi K. Tse, M.K.H. Cheung, Adaptive feedforward and feedback control schemes for sliding mode controlled power converters, IEEE Trans. Power Electron. 21 (1) (2006).
[8] A. Colombo, M.R. Jeffrey, The two-fold singularity of discontinuous vector fields, SIAM J. Appl. Dyn. Syst. 8 (2009) 624–640.
[9] A. Colombo, M.R. Jeffrey, Non-deterministic chaos and the two fold singularity in piecewise smooth flows, SIAM J. Appl. Dyn. Syst. 10 (2011) 423–451.
[10] A. Jacquemard, M.A. Teixeira, D.J. Tonon, Stability conditions in piecewise smooth dynamical systems at a two-fold singularity, J. Dyn. Control Syst. 19 (2013) 47–67.
[11] A. Jacquemard, M.A. Teixeira, D.J. Tonon, Piecewise smooth reversible dynamical systems at a two-fold singularity, Int. J. Bifurcation Chaos 22 (2012).
[12] M. di Bernardo, A. Colombo, E. Fossas, Two-fold singularity in nonsmooth electrical systems, in: Proc. IEEE International Symposium on Circuits ans Systems, 2011, pp. 2713–2716.
[13] M. di Bernardo, A. Colombo, E. Fossas, M.R. Jeffrey, Teixeira singularities in 3D switched feedback control systems, Systems Control Lett. 59 (2010) 615–622.
[14] A.A. Andronov, E.A. Leontovich, I.I. Gordon, A.G. Maier, Theory of bifurcations of dynamical systems on a plane, Israel Program for Scientific Translations, Jerusalem, 1971.
[15] Y.A. Kuznetsov, Elements of Applied Bifurcation Theory, in: Applied Mathematical Sciences, vol. 112, Springer, 1998.
[16] J.D. Meiss, Differential Dynamical Systems, in: Mathematical Modelling and Computation, vol. 1, Society for Industrial and Applied Mathematics, 2007.
[17] L. Perko, Differential Equations and Dynamical Systems, Third ed., in: Texts in Applied Mathematics, vol. 7, Springer, 2001.
[18] P. Glendinning, Stability, Instability and Chaos: An Introduction to the Teory of Nonlinear Differential Equations, Cambridge University Press, 1994.
[19] J. Llibre, E. Ponce, J. Ros, F. Torres, On the Fold-Hopf bifurcation for continuous piecewise linear differential systems with symmetry, Chaos 20 (2010).
[20] Bin Xu, Fenghong Yang, Yun Tang, Mu Lin, Homoclinic bifurcations in planar piecewise-linear systems, Discrete Dyn. Nat. Soc. 2013 (2013) 9. Article ID 732321.
[21] Liping Li, Lihong Huang, Concurrent Homoclinic bifurcation and Hopf bifurcation for a class of planar Filippov systems, J. Math. Anal. Appl. 411 (1) (2014) 83–94.
[22] D.J.W. Simpson, J.D. Meiss, Andronov–Hopf bifurcations in planar, piecewise-smooth, continuous flows, Phys. Lett. A 371 (3) (2007) 213–220.
[23] F. Dercole, F.D. Rossa, A. Colombo, Y.A. Kuznetsov, Two degenerate boundary equilibrium bifurcations in planar Filippov systems, SIAM J. Appl. Dyn. Syst. 10 (4) (2011) 1525–1553.
[24] Yu.A. Kuznetsov, S. Rinaldi, A. Gragnani, One-parameter bifurcations in planar Filippov systems, Int. J. Bifurcation Chaos 13 (8) (2003) 2157–2188.
[25] F. Battelli, M. Feckan, Bifurcation and chaos near sliding homoclinics, J. Differential Equations 248 (2010) 2227–2262.
[26] C.A. Buzzi, T. Carvalho, M.A. Teixeira, On three-parameter families of Filippov systems — the fold-saddle singularity, Int. J. Bifurcation Chaos 22 (2012).
[27] R. Cristiano, D.J. Pagano, L. Benadero, E. Ponce, Bifurcation analysis of a DC-DC bidirectional power converter operating with constant power load, Int. J. Bifurcation Chaos 26 (2016) 1630010. (18 pages).
[28] L. Benadero, R. Cristiano, D. Pagano, E. Ponce, Nonlinear analysis of interconnected power converters: A case study, IEEE J. Emerg. Sel. Top. Circuits Syst. 5 (3) (2015) 326–335.
[29] T. Carvalho, M.A. Teixeira, Basin of attraction of a cusp-fold singularity in 3D piecewise smooth vector fields, J. Math. Anal. Appl. 418 (2014) 11–30.
[30] A.P.N. Tahim, D.J. Pagano, E. Ponce, Nonlinear control of boost bidirectional converters in stand-alone dc microgrids, in: 51st IEEE Conference on Decision and Control - CDC. Maui, Hawaii, USA, 2012.
[31] L.M. Perko, Global families of limit cycles of planar analytic systems, Trans. Amer. Math. Soc. 322 (1990) 627–656.
[32] L.M. Perko, Multiple limit cycle bifurcation surfaces and global families of multiple limit cycles, J. Differential Equations 122 (1995) 89–113.
[33] A. Barreiro, J. Aracil, D.J. Pagano, Detection of attraction domains of non-linear systems using bifurcation analysis and Lyapunov functions, Internat. J. Control 75 (5) (2002) 314–327.